Cells, reagents, and mice

Twelve-week-old male wild-type C57BL/6J mice were obtained from Charles River Laboratories. Also used in this study were age-matched integrin mutant mice (L746A and Y747A knock-in mice), and their littermate controls,[1] and TNF-α KO, TNF-α–R1 KO, IL-1 α/β double KO, and IL-1RA KO mice, and their littermate controls.[2–6] P-selectin KO and E-selectin KO mice were obtained from Charles River Inc. Platelet-specific Rac1 KO mice (Pf4-Rac1 KO) were generated by mating Rac1 flox/flox mice, and Pf4-Cre transgenic mice were kindly provided from Dr. Radek Skoda (University Hospital Basel, Switzerland).[7,8] We confirmed the deletion of Rac1 in megakaryocytes and platelets from Pf4-Rac1 KO mice. All animal and recombinant DNA experiments were approved by the Institutional Animal Care and Use Committee, and strictly adhered to the guidelines for animal experiments of The University of Tokyo.

Creating chimeric mice using bone marrow transplantation

To obtain chimeric mice, bone marrow from femurs was washed with phosphate-buffered saline, and wild-type, TNF-α KO, or TNF-R1 KO bone marrow cells were intravenously transfused into lethally irradiated (9.5 Gy), 8-week-old male recipient mice (10^7 cells per recipient mouse).

Intravital microscopy and thrombus formation

To visually analyze thrombus formation in the microcirculation of the mesentery in living animals, we used *in vivo* laser injury with a visualization technique developed through modification of conventional methods.[9,10] Male mice were anesthetized by injection with urethane (1.5 g/kg), and a small incision was made so that the mesentery could be observed without being exteriorized. FITC-dextran (150 kDa [Sigma FD150] and 10 kDa [Sigma FD10S]) or Texas-Red-dextran (70 kDa, Invitrogen, D1830) was injected into mice to visualize cell dynamics, while hematoporphyrin (1.8 mg/kg in capillaries and 5 mg/kg in arterioles and arteries, Sigma H5518) was injected to produce ROS upon laser irradiation. Blood cell dynamics and thrombus production were visualized during laser excitation and ROS production (wave length 488 nm, 1.5 mW power through a 100× oil immersion objective lens (N.A.: 1.3, Nikon). ROS production was induced by laser irradiation of the entire imaging field; we did not use high-power laser irradiation of a limited area. Sequential images were obtained for 20 to 40 s at 10 to 30 frames/s using a spinning-disk confocal microscope (Yokogawa-electronics, CSU-X1) equipped with two EM-CCD cameras (iXon; Andor) or a Nikon A1R System equipped with a resonance scanning system (30 frames/s for 20 to 60 s).

To detect ROS production, the mice were administered the fluorogenic indicator 2-[6-(4'-amino) phenoxy-3H-xanthen-3-on-9-yl] benzoic acid (APF, 0.8 mg/kg, Sekisui Medical). To detect fibrinogen binding, they were administered Alexa 488-conjugated fibrinogen (10 mg/kg, human-derived, Invitrogen, F13191). To visualize the endothelial cell layer, they were administered FITC-conjugated *Griffonia simplicifolia* IB_4 isolectin (2.0 mg/kg, Vector Laboratories). To selectively visualize platelet kinetics, the mice were intravenously administered Dylight 488-conjugated anti–GPIbβ antibody (0.2 mg/kg, X488, Emfret) 15 min before the visualization experiments. The concentration of anti-GPIbβ antibody used in these experiments did not significantly affect the platelet kinetics. To visualize the nuclei of leukocytes and endothelial cells, Hoechst 33342 (2.5 mg/kg, Invitrogen) was administered. To visualize the vWF distribution in laser-injured vessels, Alexa 647-conjugated (Invitrogen) anti-vWF antibodies

(0.2mg/kg, LifeSpan BioSciences) were administrated before the visualization experiments. Changes in anti-vWF signal intensity after laser-induced thrombus formation were assessed at the endothelial cell surface (white boxes in Fig 6A) using NIS-Elements software (Nikon). To assess the effect of the EC inflammation status, in some cases we administrated TNF-α (0.5 mg/kg body weight, T7539, Sigma) and IFN-γ (0.5 mg/kg body weight, I4777, Sigma) prior to the experiment. To assess the effect of thrombin inhibition, we treated hirudin (Sigma-aldich, 94581, 1mg/kg body weight) with fluorescent dextran, and performed the in vivo imaging.

To obtain simultaneous multi-color signals using a spinning disk confocal microscope (CSU-X1), we utilized the 2nd port of the CSU-X1 and a pair of iXON EM-CCD cameras. The specimens were excited using an Ar-Kr laser (488 nm and 568 nm), and the emission signal was collected using dichroic mirrors. Red and green signals were separated by a second 565-nm dichroic mirror, and a 510-nm band-pass barrier filter was used for the green signal, while a 600-nm long pass filter was used for the red signal. Otherwise, we utilized four-color resonance scanning imaging using a Nikon A1R system equipped with 405, 488, 561, and 633 nm laser lines.

To assess the effect of platelet-activating agents, we administered thrombin (300 U/kg body weight, Sigma). To examine the effects of GPIbα blockade, we administrated a neutralizing anti-GPIbα (4 mg/kg, clone Xia.B2, Emfret) antibody. Isotype matched control rat IgGs (eBioscience) served as a negative controls. Our preliminary examinations confirmed that these antibody clones, doses and experimental durations did not change the circulating platelet counts. After laser stimulation, we did not detect changes in the *in vivo* fluorescent signal (colors or intensities) due to photo activation or other related reactions.

In our system, the networks of mesenteric vessels include substantial amounts of branching, sprouting and diameter changes, which could alter the shear stress within the examined vessels. To avoid such variation, we analyzed relatively straight vessels that had no diameter changes, sprouting or branching. In addition, by monitoring the changes in intensity of APF within the examined vessels (data not shown), we also confirmed that the relative increase in the ROS level within a vessel after laser irradiation was relatively constant in both capillaries and arterioles.

Immunohistochemistry

To analyze TNF-receptor–1 expression in mesenteric capillaries, we fixed whole mesenteric tissues using a BD Cytofix/Cyroperm kit (BD Biosciences). We then incubated the tissue with primary antibodies against TNF-R1 (1:100 dilution; Abcam) and anti-CD31 (1:100 dilution, eBioscience), followed by Alexa-conjugated secondary antibodies (Invitrogen) and Hoechst (Invitrogen). The tissues were then visualized using a Nikon A1R system.

Image analysis

To quantify platelet dynamics, sequential images (more than 20 s) were collected and analyzed as follows. Initial adherent platelets, “attachment,” were defined as those showing continuous (>2 s) interaction with the endothelium after laser-induced injury, as determined by blinded observers using IQ software (Andor) and NIS-Elements software (Nikon). This effect was expressed in terms of adherent platelet numbers per observed vascular length (usually 100 μm) per observation period (usually 5 s). To quantify thrombus “development,” platelet numbers

within thrombi were calculated as the numbers of platelets tightly adhering to vessels (>2 s) or stabilized within vessels (not moved by blood flow for >2 s) 10s and 20s after laser injury, and expressed in terms of the number of platelets per observed vascular length (usually 100 μm).

In preliminary experiments, we assessed the calculation methods for developing thrombi in our model using platelet numbers and image analysis (thrombus area) (Fig S12). Platelet number was defined as the number of platelet in a developing thrombus, while thrombus "area" was defined by fluorescent images. The results showed that there was a strong correlation between changes in platelet number and thrombus "area" during thrombus formation. Analysis of single-platelet kinetics enabled us to separately analyze the initial (sometimes transient) platelet attachment, thrombus growth, stability of the developed thrombus, and contribution of other cell types, which were all dependent on different molecular mechanisms. Collectively, these analyses are useful for assessing the multicellular kinetics of thrombus formation.

Flow chamber

Under a protocol approved by the Institutional Review Board of the University of Tokyo, blood was drawn from healthy volunteers who had no history of thrombosis and had ingested no medications. Blood was drawn into acid-citrate dextrose (ACD, Sigma) anticoagulant (85 mM sodium citrate, 104 mM glucose and 65 mM citric acid). To isolate platelets, the whole blood was centrifuged at 150 g for 15 min at room temperature to obtain platelet-rich plasma (PRP). The PRP were washed with twice with Tyrode buffer (138 mM sodium chloride, 5.5 mM glucose, 12 mM sodium bicarbonate, 2.9 mM potassium chloride, and 0.36 mM dibasic sodium phosphate, pH 7.4) and resuspended in Ca^{2+} Mg^{2+}-free Tyrode buffer. The platelets were then stained with 5 μM tetramethylrhodamine ethyl ester (Invitrogen) for 15 min, washed, and used for flow chamber analysis. The details were previously described.[11]

Human umbilical vein endothelial cells (HUVEC) were maintained in endothelial growth medium and fetal bovine serum (10%) until confluent in custom-made chambers for flow analysis. The cells were treated with small interference (si-) RNA targeting TNF-R1 (si–TNF-R1, Darmacon) or control scrambled si-RNA (Darmacon) for 48 h prior to the experiments. Treatment with recombinant human TNF-α (rTNFα) (24 h, 10 ng/ml, Sigma) was also carried out.

We analyzed platelet attachment to cultured HUVECs under high shear flow conditions using a BioFlux 200 system (Fluxion). The cell culture chamber was connected to a microfluidic device, and after perfusion for 5 min with Tyrode buffer containing stained platelets at 200 dynes/cm^2, the platelets adhering to the HUVECs were visualized in 10-μm–thick stacks of images using confocal microscopy (Nikon A1R). The numbers of adherent platelets were counted by blinded observers.

FACS analysis of adhesion molecules and vWF on HUVECs and mouse platelets

Cell adhesion molecules and surface vWF were analyzed using mouse platelets and cultured HUVECs. Blood from 12-week-old male wild-type C57BL/6J mice, TNF-α KO, and TNF-R1 KO was drawn into ACD anticoagulant, after which washed platelets were obtained as described, and resuspended in phosphate-buffered saline with 3% fetal bovine serum. HUVECs were cultured until confluent, harvested and analyzed. Some cells were treated with hematoporphyrin

(1mM, HP, as a source of O_2^-, Sigma), and stimulated by laser irradiation (488 nm laser, 1.5 mW power at objective lens, irradiation of a 30-µl volume of cell suspensions for 20 min) to induced ROS production for 20 m prior to the incubation with antibodies. Some HUVECs were treated with si-RNA targeting TNF-R1 (si–TNF-R1, Darmacon) or with control scrambled si-RNA (si-CTRL, Darmacon) 48 h prior to the experiments. Other cells were treated with H_2O_2 (1 mM, Sigma) and/or N-acetylcysteine (100 µM, Sigma, NAC) for 20 sec or 20 min. The isolated cells were then incubated with labeled specific antibodies or isotype-matched control antibodies and analyzed by flow cytometry using a Canto II flow cytometer (Becton Dickinson) and FlowJo 7.2.2. software (Tomy Digital Biology). We identified platelets using PE-Cy7 labeled (MWReg30, eBioscience) and eFluor450-labeled (MWReg30, eBioscience) anti-CD41 antibodies. Other antibodies used for HUVECs were anti-CD54 (ICAM-1, HA58, eBioscience), anti-CD62E (P2H3, eBioscience), anti-CD62P (AK4, eBioscience), anti-CD106 (VCAM-1, 51-10C9, BD Pharmingen), and anti-vWF (4F9, Abcam). The antibodies used with mouse platelets were anti-CD42 (GPIbα, Xia.G5, Emfret), anti-CD42a (GPIX, Xia.B4, Emfret), anti-CD42c (GPIbβ, Xia.C3, Emfret), anti-CD49e (integrin α5, Tap.A12, Emfret), anti-CD61 (GPIIIa, integrin β3, Luc.H11), anti-CD62P (Wug.E9, Emfret), anti-GPIIbIIIa (JON/A, Emfret), and anti-GPVI (JAQ1, Emfret).

Statistics

Statistical analysis was performed using JMP 8.0 (SAS) software. We expressed the results as means ± S.E.M. The statistical significance of differences between two groups was assessed using Student's t-tests. Differences between more than two groups were evaluated using ANOVA followed by post-hoc Bonferroni tests. We examined correlations using the Pearson correlation coefficient test. Values of $P < 0.05$ were considered significant.

REFERENCES

1. Petrich BG, Fogelstrand P, Partridge AW, et al. The antithrombotic potential of selective blockade of talin-dependent integrin alpha IIb beta 3 (platelet GPIIb-IIIa) activation. *J Clin Invest*. 2007;117:2250–2259.
2. Horai R, Asano M, Sudo K, et al. Production of mice deficient in genes for interleukin (IL)-1alpha, IL-1beta, IL-1alpha/beta, and IL-1 receptor antagonist shows that IL-1beta is crucial in turpentine-induced fever development and glucocorticoid secretion. *J Exp Med*. 1998;187:1463–1475.
3. Taniguchi T, Takata M, Ikeda A, Momotani E, Sekikawa K. Failure of germinal center formation and impairment of response to endotoxin in tumor necrosis factor alpha-deficient mice. *Lab Invest*. 1997;77:647–658.
4. Pfeffer K, Matsuyama T, Kundig TM, et al. Mice deficient for the 55 kd tumor necrosis factor receptor are resistant to endotoxic shock, yet succumb to L. monocytogenes infection. *Cell*. 1993;73:457–467.
5. Suzuki Y, Mogami H, Ihara H, Urano T. Unique secretory dynamics of tissue plasminogen activator and its modulation by plasminogen activator inhibitor-1 in vascular endothelial cells. *Blood*. 2009;113:470–478.
6. Zhao BQ, Ikeda Y, Ihara H, et al. Essential role of endogenous tissue plasminogen activator through matrix metalloproteinase 9 induction and expression on heparin-produced cerebral hemorrhage after cerebral ischemia in mice. *Blood*. 2004;103:2610–2616.

7. Kassai H, Terashima T, Fukaya M, et al. Rac1 in cortical projection neurons is selectively required for midline crossing of commissural axonal formation. *Eur J Neurosci*. 2008;28:257–267.
8. Tiedt R, Schomber T, Hao-Shen H, Skoda RC. Pf4-Cre transgenic mice allow the generation of lineage-restricted gene knockouts for studying megakaryocyte and platelet function in vivo. *Blood*. 2007;109:1503–1506.
9. Nishimura S, Manabe I, Nagasaki M, et al. In vivo imaging in mice reveals local cell dynamics and inflammation in obese adipose tissue. *J Clin Invest*. 2008;118:710–721.
10. Takizawa H, Nishimura S, Takayama N, et al. Lnk regulates integrin alphaIIbbeta3 outside-in signaling in mouse platelets, leading to stabilization of thrombus development in vivo. *J Clin Invest*. 2010;120:179–190.
11. Dong JF, Moake JL, Bernardo A, et al. ADAMTS-13 metalloprotease interacts with the endothelial cell-derived ultra-large von Willebrand factor. *J Biol Chem*. 2003;278:29633–29639.

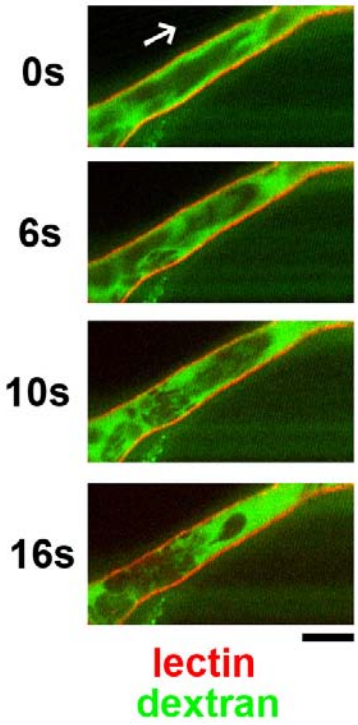

Figure S1. Thrombus formation by discoid platelets on intact endothelium after laser/ROS-induced injury visualized with lectin staining of the endothelium
The endothelial cell layer was visualized using fluorescent *Griffonia simplicifolia* IB_4 isolectin (red) and dextran (green) before and after laser injury. Note that the thrombus developed on the undisrupted endothelium. The white arrow shows the direction of blood flow. Scale bar is 10 µm.

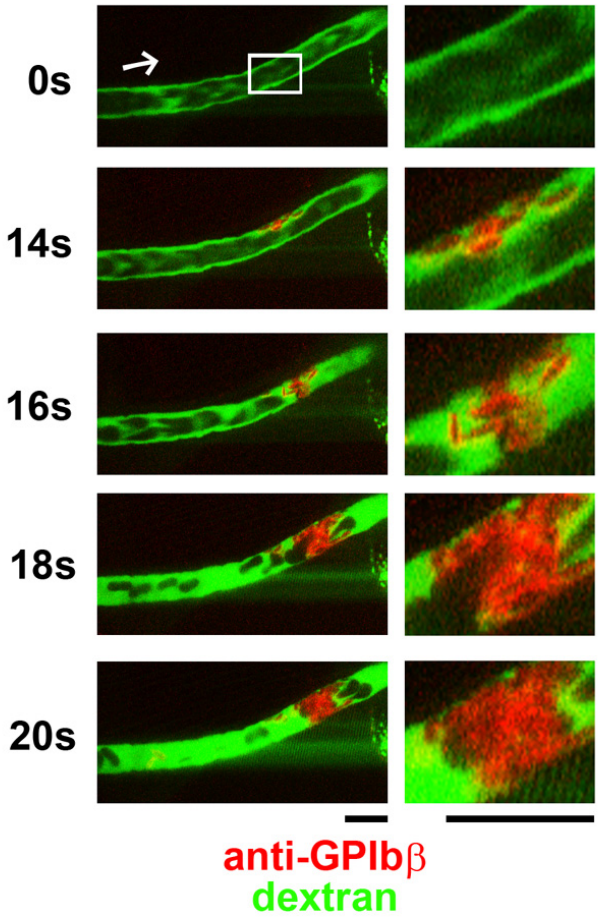

Figure S2. Thrombi formed in response to laser/ROS-induced injury are mainly composed of platelets

To define the cell population within thrombi after laser/ROS-induced injury, we stained the platelets using an anti–GPIb-β antibody. We observed that almost all of the cells within the developed thrombi were platelets. Scale bar is 10 μm.

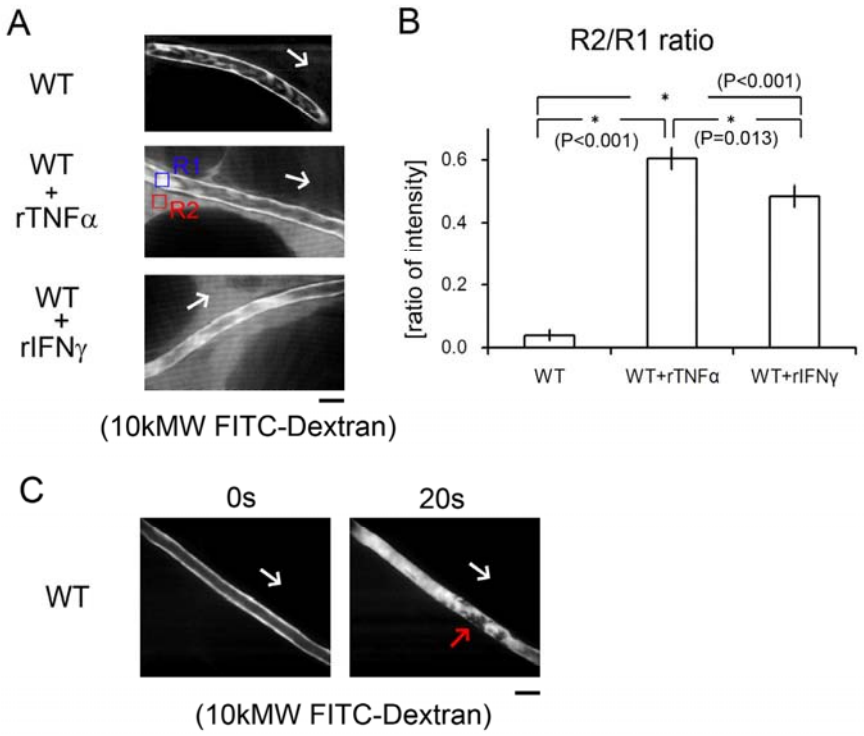

Figure S3. Extravasation of fluorescent dextran in TNF-α– and IFN-γ–treated mice, and its absence in wild-type mice, even after laser injury

To confirm that the EC layer was not disrupted in our thrombosis models, we administered small (10 kDa) FITC-Dextran to 12-week-old wild-type mice. Some mice were treated with TNF-α (0.5 mg/kg) or IFN-γ, (0.5 mg/kg) prior to the experiments to visualize the effect of EC inflammation status. (A) *In vivo* imaging of mesenteric capillaries under basal conditions (without laser injury) in control wild-type mice (WT), recombinant TNF-α–treated (WT+rTNFα) mice and recombinant IFN-γ–treated (WT+rIFNγ) mice. White arrows indicate the direction of blood flow, the blue box (R1) indicates the ROI (region of interest) for intravascular signals, and the red box (R2) indicates the ROI for signals from the stromal space. Note the extravasation of FITC-dextran to the stromal space in cytokine-treated mice, which was not seen in wild-type mice. (B) R2/R1 ratios showing the extravasation of fluorescent dextran in cytokine-treated mice (n=20 vessels from five animals for each group). (C) *In vivo* imaging of mesenteric capillaries 20 s after laser injury in control mice administered 10 kDa FITC-dextran. Note the absence of extravasation in laser-injured capillaries in wild-type mice, indicating that in our thrombosis model, the EC layer is undisrupted. Scale bars are10 μm. Asterisks indicate statistical significance ($P<0.05$).

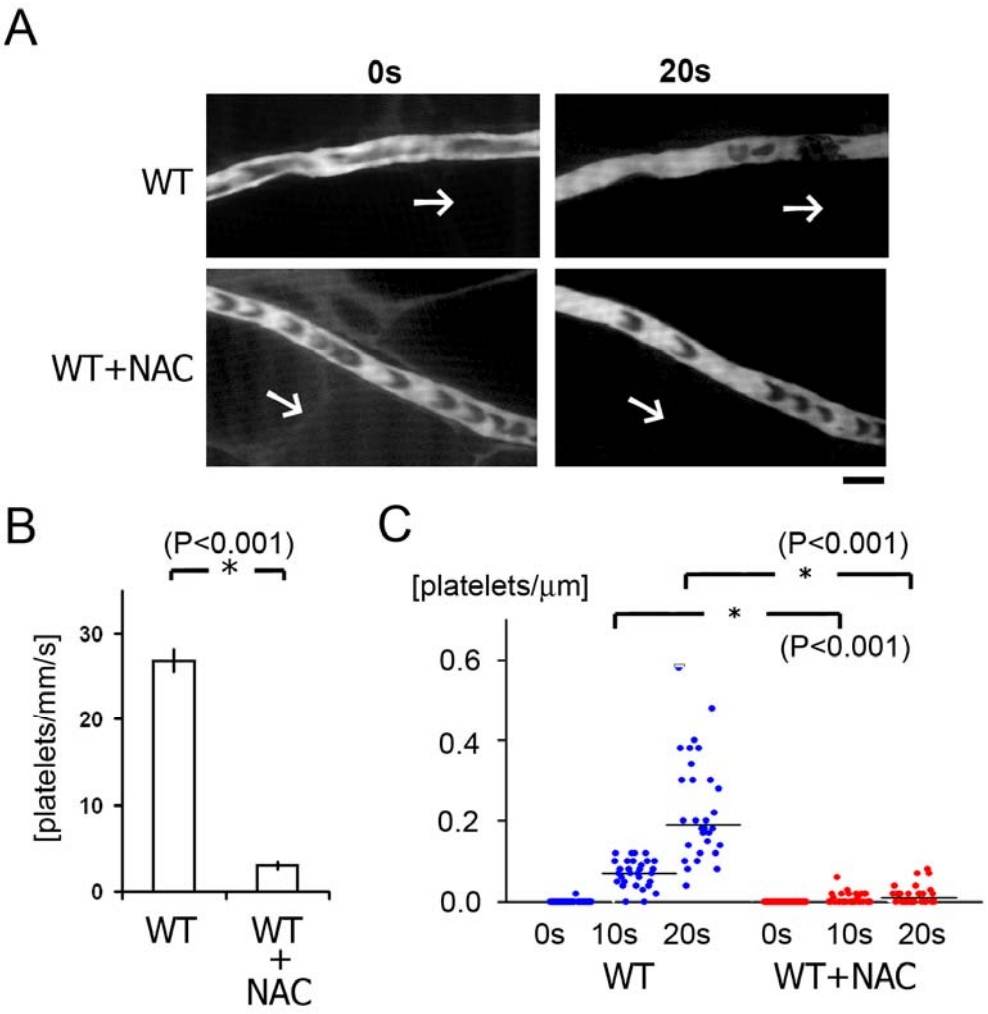

Figure S4. N-acetylcysteine completely block platelet aggregation after laser/ROS-induced injury

To assess the effect of the ROS scavenger N-acetylcysteine (NAC), we performed laser/ROS-induced injury experiments using wild-type (WT) mice and mice treated with NAC (2 mg/g body weight). (A) NAC treatment almost completely inhibited platelet attachment to vessel walls and thrombus development after laser/ROS-induced injury. Representative *in vivo* images are shown. The numbers of platelets that attached to the vessel wall during the first 10 s after injury (B) and subsequent thrombus development (C) are shown. White arrows indicate the direction of blood flow. Scale bar is 10 μm.

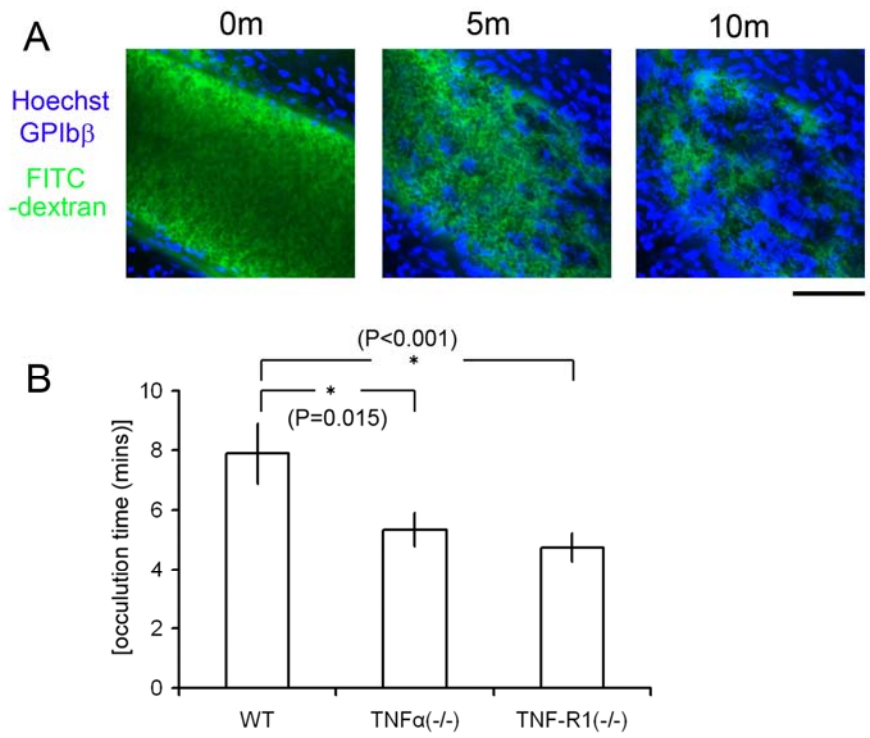

Figure S5. Our *in vivo* imaging technique can be applied to femoral arteries, and elucidate the impaired thrombus formation in large-sized artery models

We also performed thrombus formation using high dose of hematoporphyrin (5 mg/kg) in femoral arteries, and examined the occulusion time by the developed thrombus. (A) *In vivo* imaging of femoral artery occulusion induced by laser-thrombi in 12-week-old WT mice. Thrombus was visualized by Hoechst (leukocyte) and anti-GPIbβ (platelets). We confirmed that this technique can be applied to large-sized arteries for evaluation of thrombosis formation. (B) Occulusion time of same aged male TNF-α KO, TNF-R1 KO mice and WT control of femoral arteries. We also observed the impaired thrombus formation in large-sized artery levels in inflammatory cytokine KO mice White arrows indicate the direction of blood flow. Scale bar is 100 μm (n=20 vessels from five animals in each group) Asterisks indicate statistical significance ($P<0.05$).

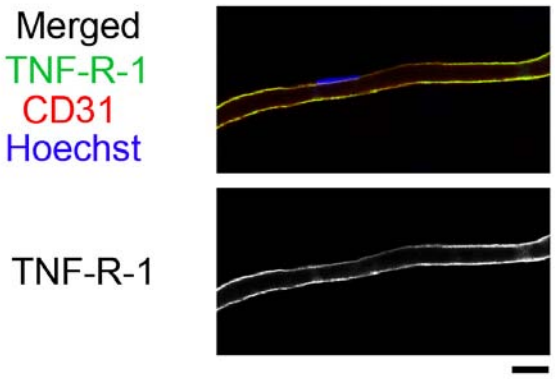

Figure S6. Immunohistochemical study of TNF-R1 in mesenteric capillaries
Immunohistochemical study of TNF-R1 (green) in mesenteric capillaries of 12-week-old wild-type mice. The vessels were staining with anti-CD31 antibody (red) for vasculature and Hoechst (blue) for nuclei. Scale bar is10 µm.

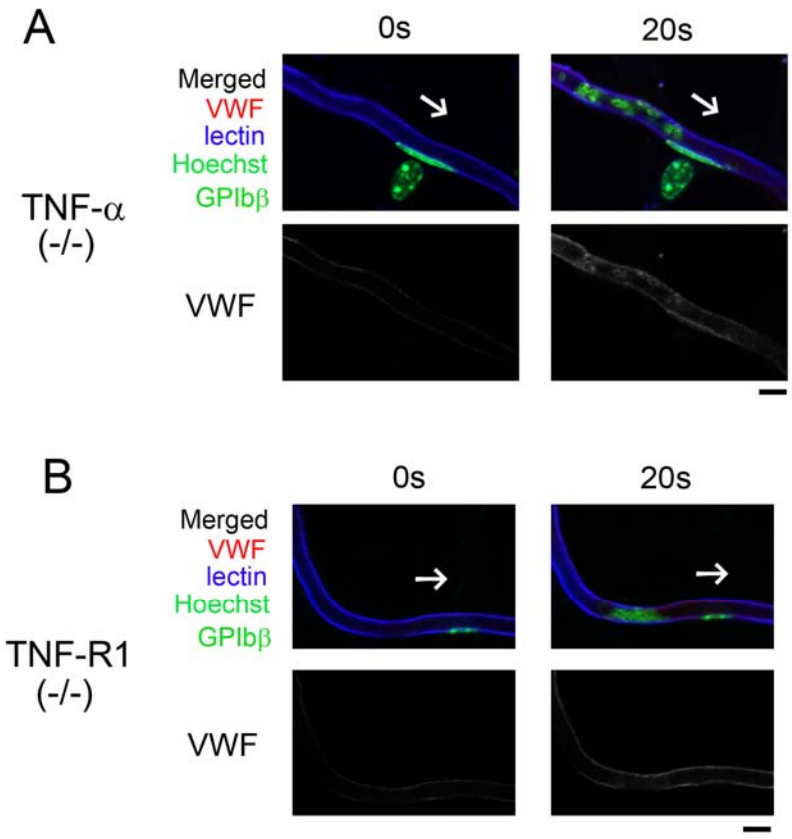

Figure S7. vWF expression on the endothelial cell surface after laser/ROS-induced injury is decreased in TNF-α and TNF-R1 knockout mice

(A, B) *In vivo* imaging of vWF mobilization onto the endothelial cell surface in TNF-α and TNF-R1 knockout mice. Fluorescent anti-vWF antibody (red) was administrated and visualized before and after laser/ROS-induced injury. vWF was expressed on the endothelial cell surface within the affected vessel after laser/ROS-induced injury, but its expression was diminished in both knockout mice, as compared to the wild-type (Fig 6A). Quantification of the vWF signal intensity is shown in Figure 6B. The cells were also co-stained with lectin (blue, vasculature), anti-GPIbβ (green, platelets) and Hoechst (green, nucleus). Arrows indicate the direction of blood flow. Scale bar is 10 μm.

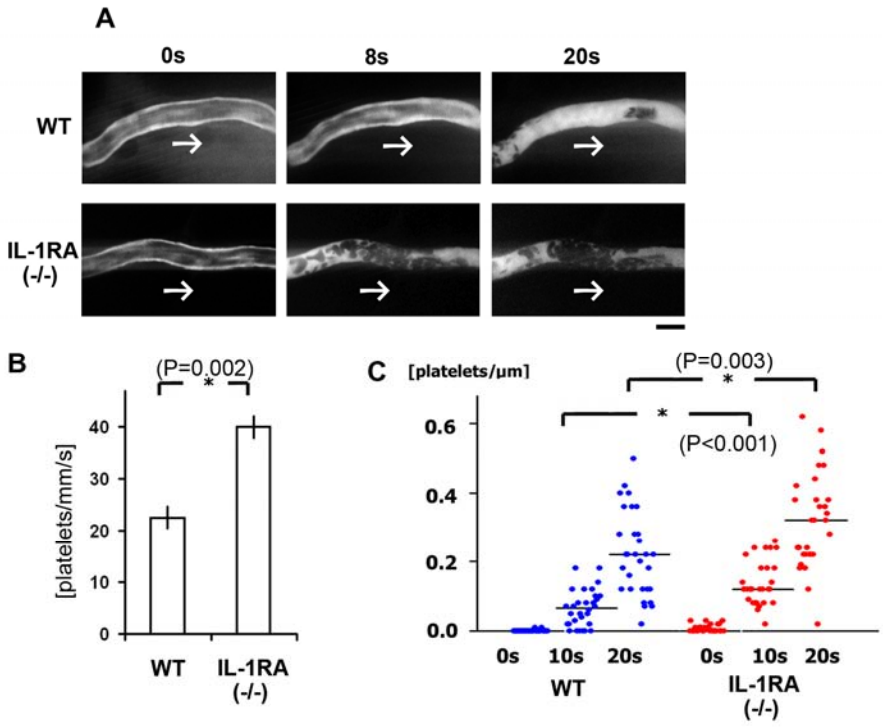

Figure S8. IL-1 receptor antagonist-deficient mice showed enhanced platelet attachment to vessel walls and thrombus development after laser/ROS-induced injury

To assess the effect of IL-1 receptor antagonist (IL-1RA) deficiency on thrombus formation, we performed laser/ROS-induced injury experiments using twelve-week-old male IL-1RA knockout mice and their wild-type (WT) littermates. (A) IL-1RA deficiency led to enhanced platelet attachment to vessel walls and thrombus development after laser/ROS-induced injury. The numbers of platelets that attached to the vessel wall during the first 10 s after injury (B) and subsequent thrombus development (C) are shown. White arrows indicate the direction of blood flow. Scale bar is 10 μm.

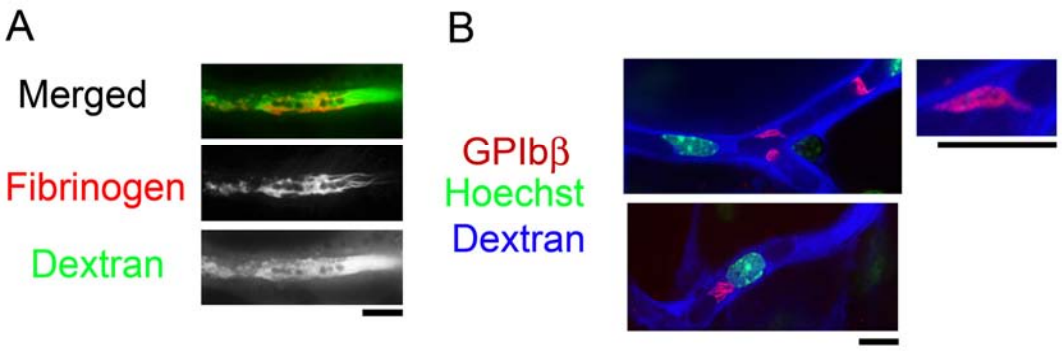

Figure S9. Thrombin administration induces thrombosis with fibrinogen network formation, platelet deformation and leukocyte plugging
(A) Thrombus formation following thrombin administration (300 U/kg body weight). Note the filamentous fibrinogen network. (B) Formation of a thrombus composed of multiple cell types after thrombin administration. Platelets, erythrocytes and leukocyte nuclei were visualized using anti–GPIb-β antibody (green), dextran (red) and Hoechst 33342 (blue), respectively. Platelets showed marked deformation. All scale bars are 10 μm.

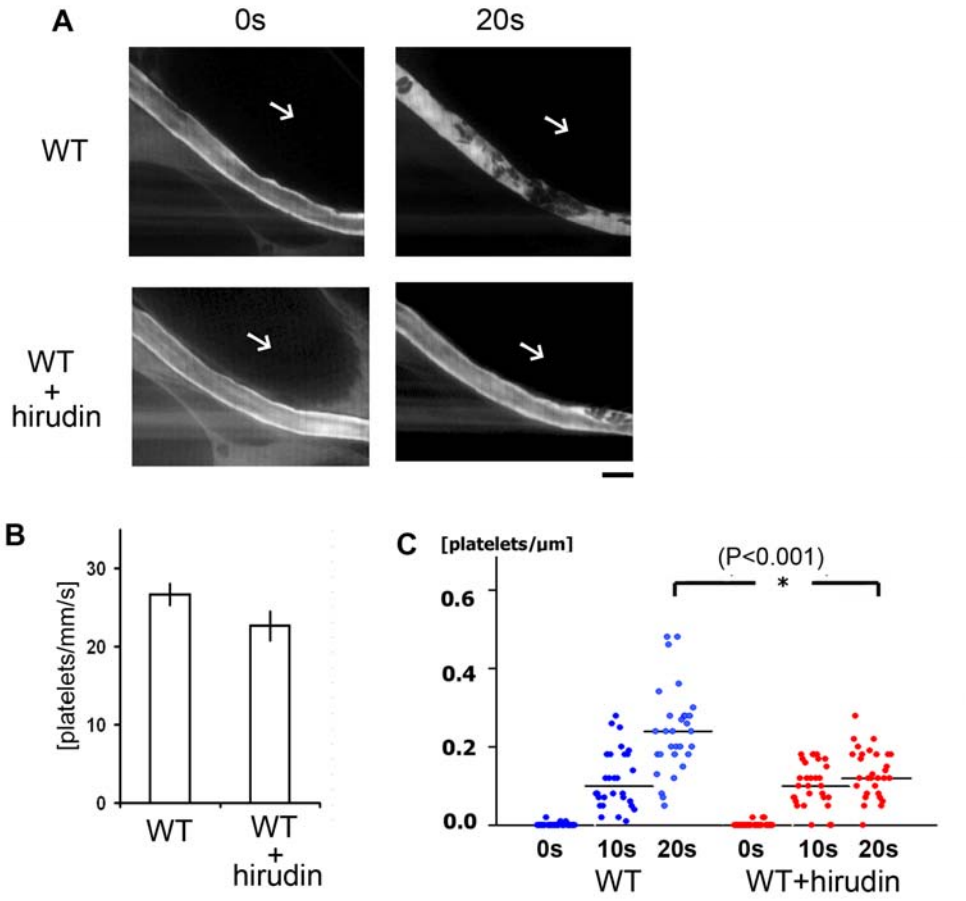

Figure S10. Thrombin inhibitor (hirudin) impaired thrombus development in late phase, but not initial platelet attachment after laser injuries

To assess the effect of thrombin inhibitor (hirudin, 1mg/kg body weight), we performed laser/ROS-induced injury experiments using twelve-week-old male wild type mice and those treated with hirudin. (A) *In vivo* imaging revealed hirudin treatment impaired the thrombus development 20s after laser/ROS-induced injury. (B) Quantification of initial attachment revealed that hirudin treatment did not affect the number of initial attached platelets to the vessel wall during the first 10 s after injury. (C) Calculations of subsequent thrombus development showed the impaired thrombus formation in late phase by hirudin treatment. White arrows indicate the direction of blood flow. Scale bar is 10 μm (n=30 vessels from five animals in each group).

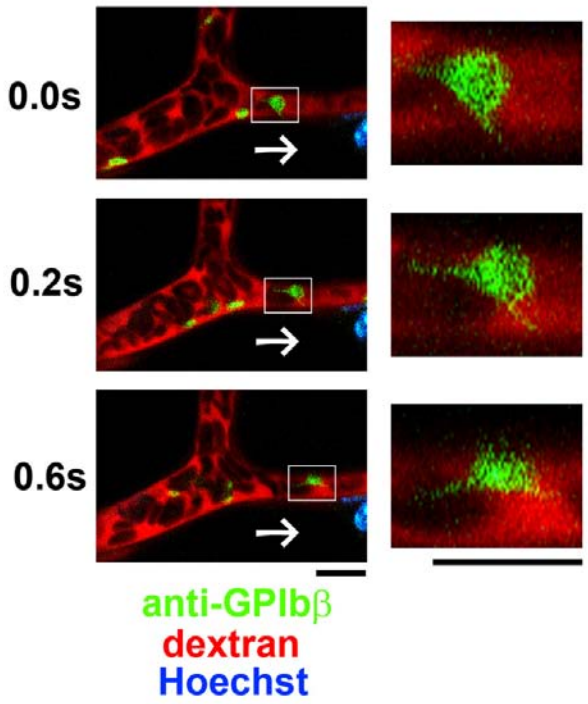

Figure S11. *In vivo* imaging of deformed platelets after strong laser irradiation
We detected deformed platelets in the circulating blood after high-power laser irradiation (wave length 488 nm, 5 mW power at the objective lens). Multicolor *in vivo* imaging using Hoechst 33342 (blue), anti–GPIb-β antibody (green), and fluorescent dextran (dextran) to stain nuclei, platelets and erythrocytes, respectively. White arrows show the direction of blood flow, and white boxes show a circulating deformed platelet. Scale bars are 10 μm.

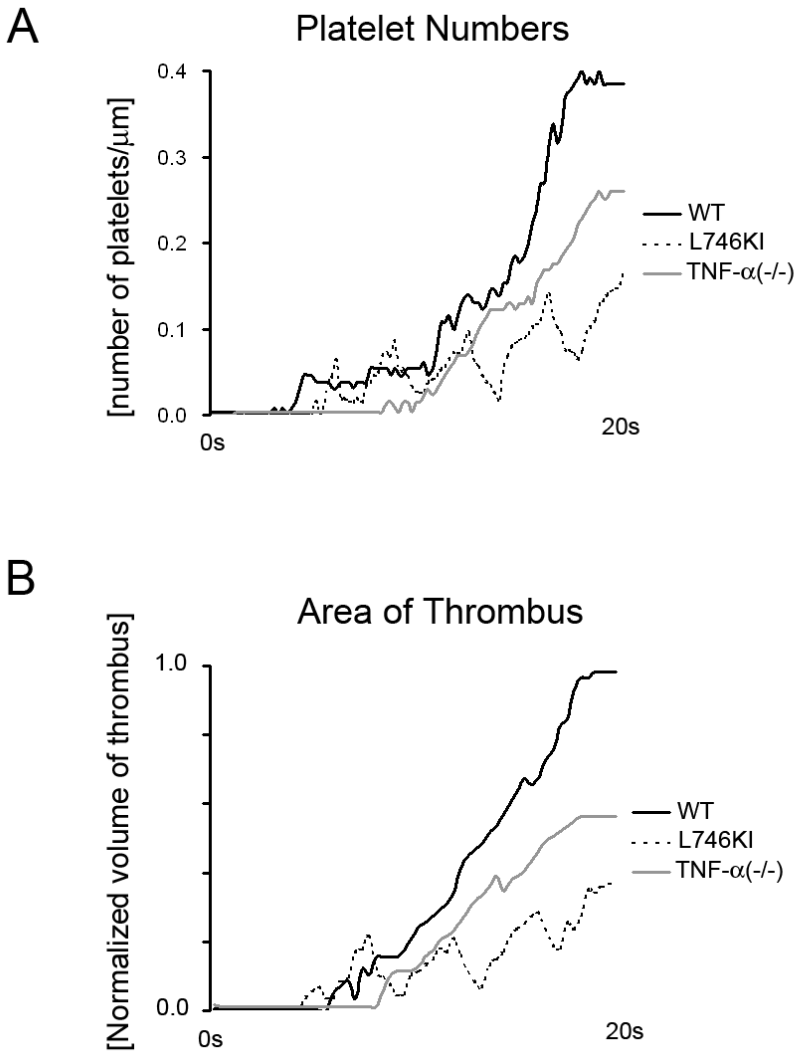

Figure S12. Changes in platelet number and thrombus area during thrombus development
Representative curves showing the platelet numbers and thrombus "area" after laser/ROS-induced injury in mesenteric capillaries of 12-week-old male wild-type (WT, black line), TNF-α KO (gray line) and L746 KI (dotted line) mice. (A) Platelet number was defined as the numbers of platelets in a developing thrombus. (B) Thrombus "area" was defined by visualizing the thrombus using fluorescent dextran and normalized to the peak value 20 s after laser-induced injury in WT mice. Note that in all of the mice there is a strong correlation between changes in platelet number and thrombus "area" during thrombus formation.